Chapter 9

Energy Storage in Concrete Bed

Adeyanju Anthony Ademola

Additional information is available at the end of the chapter

http://dx.doi.org/10.5772/intechopen.77205

Abstract

The energy storage ability and temperature arrangement of a concrete bed which was charged and discharged at the same time was examined mathematically in this research. This was carried out by modeling a single globe-shaped concrete which was utilized to simulate a series of points along the concrete bed axis. Charging and discharging mode of the system were compared for 0.0094, 0.013, and 0.019 m^3/s air flow rates. Higher change in temperature response was detected between the charging and fluid to solid heat transfer process at the inception of the concrete bed and the heat gain by the cool air flowing inside the copper tube was fairly high. The analysis of energy storage efficiency was also carried out and it was noticed that the globe-shaped concrete of 0.11 m diameter has the highest storage efficiency of 60.5% at 0.013 m^3/s airflow rate.

Keywords: energy storage, heat transfer model, globe-shaped concrete, charging and discharging

1. Introduction

Heat can be transferred in a concrete bed through the following means: (i) heat transfer by convection from the bed wall to the fluid flowing inside the bed; (ii) heat transfer by convection from the globe-shaped concretes to fluid flowing in the bed, and this is known as fluid to particle mode; (iii) heat transfer by conduction from the bed walls to the globe-shaped concretes; (iv) heat transfer by conduction from one globe-shaped concrete to another, and this is known as particle to particle mode; (v) heat transfer by radiation; and (vi) heat transfer through fluid mixture [1]. The modes are as shown in **Figure 1**.

The particle to particle conduction mode can be further analyzed in axial and radial directions. Heat transfer through radiation mode will actually be important at higher temperatures.

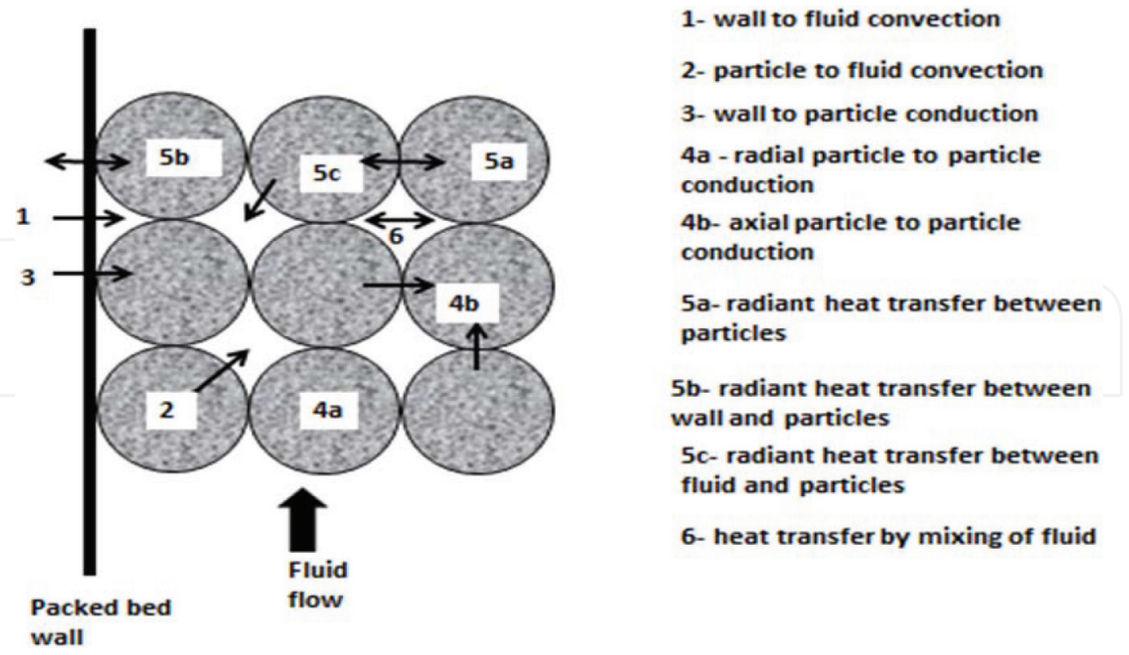

Figure 1. Schematic showing the modes of heat transfers in concrete bed.

Practically, it is found that two or three of the modes discussed earlier on can occur simultaneously. For example, the conduction between the particles may be affected by the convection between the particles and the fluid. This interaction among the different modes is one of the main reasons for the difficulty in correlating the total heat transfer and analyzing the experimental data in this field [2].

This research carried out numerically the temperature distribution in a concrete bed and also looked into the ability of a concrete bed to store energy simultaneously.

2. Review of literature

Anzelius [3] is the first author to publish a paper in heat transfer through packed beds but Schumann [4] is usually the first reference cited in most literature [1]. Both authors made some assumptions in order to find solution to equations that guide heat transfer for an incompressible fluids passing uniformly through a bed of solid particles with perfect conductivity. The following are the heat transfer equations derived for the system:

$$\frac{(T_s - T_{s,0})}{(T_s - T_{s,0})} = 1 - e^{-Y-Z}\Sigma Y^n M^n(yz) = e^{-Y-Z}\Sigma Z^n M_n \tag{1}$$

$$\frac{(T_f - T_s)}{(T_{f,0} - T_{s,0})} = 1 - e^{-Y-Z}\Sigma[Y^n M^n(yz)] = e^{-Y-Z}\Sigma[Z^n M_n(yz)] \tag{2}$$

where T_s is the solid temperature, T_f is the temperature of fluid and Y and Z are dimensionless quantities. Eqs. (1) and (2) was solved simultaneously and the result were analyzed graphically to form Schumann curves. Knowing the outlet air and bed temperature, these curves can be

used to determine the volumetric heat transfer coefficients and also the heat transfer coefficients of a packed bed undergoing heat exchange with a fluid provided the following conditions which were the simplifying assumptions made by Schumann were satisfied:

1. Due to the infinitesimal nature of the solid particles, resistance to heat transfer was so small.
2. Resistance to conduction heat transfer in the fluid was so small.
3. At any section of the bed, the heat transfer rate from fluid to solid or from solid to fluid was directly proportional to their average difference in temperature between the solid and fluid within the bed.
4. The transport properties of solid and fluid were not dependent on temperature, for example the density.

Furnas [5] utilized and expanded the Schumann curves to cover more range of temperatures and suggested an empirical relation for determination of heat transfer coefficient as shown in Eq. (3):

$$h_v = \frac{BG^{0.7}T^{0.3}10^{1.68\varepsilon - 3.56\ \varepsilon 2}}{{d_p}^{0.9}} \tag{3}$$

where, h_v is the volumetric heat transfer coefficient. B is a constant dependent on the bed material, G is the mass velocity of the fluid, T is the average air temperature, d_p is the particle diameter and ε is the porosity.

Saunders and Ford [6] utilized dimensional analysis to derive correlations to calculate heat transfer coefficient. The research was for spherical shaped alone and the application is not suitable for other solid particle geometries.

Another correlation for the determination of heat transfer coefficient between gases and randomly packed solid spheres was postulated by Kays and London [7]. Using the Colburn j-factor, the relationship was written as:

$$j_h = \frac{0.23}{{Re_p}^{0.3}} \tag{4}$$

$$\text{where, } j_h = St.Pr^{2/3}$$

$$200 < Re_p < 50,000 \text{ and } 0.37 < \varepsilon < 0.39$$

Löf and Hawley [8] studied heat transfer between air and packed bed of granitic gravel. Unsteady state heat transfer coefficients were correlated with the air mass velocity and particle diameter to obtain the equation:

$$h = 0.652\ \left(G/d_p\right)^{0.7} \tag{5}$$

This was calculated for 8 mm < d_p < 33 mm; 50 < Rep 500 and temperature range of 311–394 K. The author reached a conclusion that the temperature of the entering air had no appreciable effect on the hat transfer coefficient.

Leva et al. [9] studied and analyzed heat transfer coefficient between smooth spheres of low thermal conductivities and fluids (air and carbon dioxide) in packed beds and tubes of 50.8 and 6.4 mm diameters, respectively. The ratio of particles to tube diameters was varied from 0.08 to 0.27; gas flow rate was of Reynolds number range 250 to 3000. Correlation of film coefficient was determined as:

$$h = 3.50 \left(\frac{k}{D_t}\right) e^{-4.6\frac{Dp}{Dt}\left(\frac{DpG}{\mu}\right)0.7} \tag{6a}$$

which is approximately:

$$h = 0.40\ (k/D_t)\ \left(DpG/\mu\right)\ 0.7 \tag{6b}$$

$$\text{Or, } N = 0.4\ Re^{0.7} \tag{6c}$$

Maximum film coefficient was predicted and verified at a value of Dp/Dt equal 0.153.

Riaz [10] and Jefferson [11] studied the dynamic behavior of beds undergoing heat exchange with air using single and two phased modes. By incorporating factors of axial bed conduction and intra-particle resistance, which Schumann ignored, the heat transfer coefficients were evaluated and found to be 1 + Bi/5 times smaller than those predicted using Schumann curves.

Ball [12], Norton [13], Meek [14], Bradshaw and Meyers [15], Harker and Martyn [16] and also, Bouguettaia and Harker [17] have all researched on various packed beds using air and other gases as fluids and have developed correlations involving the heat transfer coefficient.

3. Methodology

3.1. Heat transfer model for a globe-shaped concrete bed

The modeling of heat transfer in a concrete bed was carried out mathematically. It was done through a single globe-shaped concrete which was simulated mathematically to represent series of points along the concrete bed axis.

A one dimensional finite difference formulation was used in modeling the single globe-shaped concrete material, where heat conduction to neighboring globe-shaped concrete was ignored.

Using this assumption reduced the globe-shaped concrete model to that of an isolated sphere in cross flow, where the total surface area of the sphere was exposed to convection. Also, the thermal properties of the materials within the bed accounted for temperature dependence.

3.2. Finite difference formulation of a single spherical shaped concrete material

Since conduction to other globe-shaped concrete has been neglected, the geometry allows the concrete to be reduced to one dimension along its radius.

A finite difference method was utilized to model this mathematically, [18]. For this approach, the globe-shaped concrete can be characterized by three different nodal equations:

i. a general, interior node

ii. the center node

iii. the surface node

All exposed to convection as shown in **Figure 2**.

For the general and interior node within the globe-shaped concrete model, the conduction equation for $T_{(r,t)}$ is:

$$\rho_c C_c \frac{\partial T}{\partial t} = \frac{1}{r^2}\frac{\partial}{\partial r}\left(K_c r^2 \frac{\partial T}{\partial r}\right) + \dot{q}_{(r,t)} \tag{7}$$

where C_c = specific heat of concrete.

K_c = thermal conductivity of concrete.

$\dot{q}$ = heat generation.

And this equation was represented in finite difference form.

The specific heat, thermal conductivity, and the heat generation, are temperature dependent and varied with the temperature along the radial direction.

Because the thermal properties are functions of temperature, and consequently functions of the globe-shaped concrete radius, the finite difference equations are derived by the volume integration over a finite difference node.

Multiplying Eq. (7) by r^2 and integrating both sides of the equation from $r_n - \Delta r/2$ to $r_n + \Delta r/2$ resulted to:

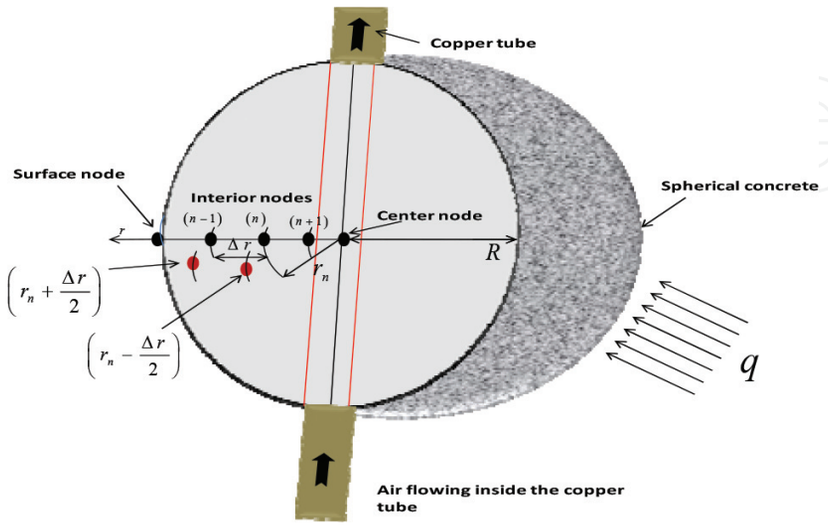

Figure 2. Schematic showing the cross-section of the globe-shaped concrete materials imbedded with copper tube.

$$\rho_c C_c \frac{\partial T}{\partial t} \int_{r_{n-\frac{\Delta r}{2}}}^{r_{n+\frac{\Delta r}{2}}} r^2 dr = \int_{r_{n-\frac{\Delta r}{2}}}^{r_{n+\frac{\Delta r}{2}}} \frac{\partial}{\partial r}\left(K_c r^2 \frac{\partial T}{\partial r}\right) dr + \int_{r_{n-\frac{\Delta r}{2}}}^{r_{n+\frac{\Delta r}{2}}} r^2 \dot{q}_{(r,t)} dr \tag{8}$$

The specific heat was assumed constant with respect to *r,* and therefore brought outside the integral.

By evaluating the integrals in Eq. (8) and representing the derivatives in finite difference form using the fully implicit method gives:

$$\rho_c C_c \left(\frac{T_n^{Z+1} - T_n^Z}{\Delta t}\right)\left(\frac{r_{n^+}^3 - r_{n^-}^3}{3}\right) = \int_{r_{n-\frac{\Delta r}{2}}}^{r_{n+\frac{\Delta r}{2}}} 2K_c r dT + \dot{q} \int_{r_{n-\frac{\Delta r}{2}}}^{r_{n+\frac{\Delta r}{2}}} r^2 dr \tag{9}$$

$$\rho_c C_c \left(\frac{T_n^{Z+1} - T_n^Z}{\Delta t}\right)\left(\frac{r_{n^+}^3 - r_{n^-}^3}{3}\right) = \left[\frac{2K_c r^2}{2}\frac{dT}{\Delta r}\right]_{r_{n-\frac{\Delta r}{2}}}^{r_{n+\frac{\Delta r}{2}}} + \dot{q}_n \left[\frac{r^3}{3}\right]_{r_{n-\frac{\Delta r}{2}}}^{r_{n+\frac{\Delta r}{2}}} \tag{10}$$

$$\begin{aligned}\rho_c C_c \left(\frac{T_n^{Z+1} - T_n^Z}{\Delta t}\right)\left(\frac{r_{n^+}^3 - r_{n^-}^3}{3}\right) &= K_{c(n^+)} r_{n^+}^2 \left(\frac{T_{n+1}^{Z+1} - T_n^{Z+1}}{\Delta r}\right) - \\ K_{c(n^-)} r_{n^-}^2 \left(\frac{T_n^{Z+1} - T_{n-1}^{Z+1}}{\Delta r}\right) &+ q_n \left[\frac{r_{n^+}^3 - r_{n^-}^3}{3}\right]_{r_{n-\frac{\Delta r}{2}}}^{r_{n+\frac{\Delta r}{2}}}\end{aligned} \tag{11}$$

where T_n^Z and T_n^{Z+1} indicate temperatures for an arbitrary node at times t^Z and t^{Z+1} respectively.

Also,

$$\mathrm{W}_n = \mathrm{W}\,\mathrm{at}\,T_n^{Z+1} \tag{12}$$

and,

$$K_{n^+} = \frac{K\left[T_{n+1}^{Z+1} + K\right]}{2}, \mathrm{at}\,T_n^{Z+1} \tag{13}$$

also,

$$r_{n^+} = r_n + \frac{\Delta r}{2} \tag{14}$$

$$r_{n^-} = r_n - \frac{\Delta r}{2} \tag{15}$$

Eq. (11) can be rearranged and solved for T_n^Z plus a known quantity which resulted to:

$$\rho_c C_c\left(\frac{T_n^{Z+1}-T_n^Z}{\Delta t}\right)=\frac{3K_{c(n^+)}r_{n^+}^2}{r_{n^+}^3-r_{n^-}^3}\left(\frac{T_{n+1}^{Z+1}-T_n^{Z+1}}{\Delta r}\right)- \frac{3K_{c(n^-)}r_{n^-}^2}{r_{n^+}^3-r_{n^-}^3}\left(\frac{T_n^{Z+1}-T_{n-1}^{Z+1}}{\Delta r}\right)+\dot{q}_n\left[\frac{3r_{n^+}^3-r_{n^-}^3}{3r_{n^+}^3-r_{n^-}^3}\right] \tag{16}$$

$$\rho_c C_c\frac{T_n^{Z+1}}{\Delta t}-\rho_c C_c\frac{T_n^Z}{\Delta t}=\frac{3K_{c(n^+)}r_{n^+}^2}{r_{n^+}^3-r_{n^-}^3}\left(\frac{T_{n+1}^{Z+1}-T_n^{Z+1}}{\Delta r}\right)- \frac{3K_{c(n^-)}r_{n^-}^2}{r_{n^+}^3-r_{n^-}^3}\left(\frac{T_n^{Z+1}-T_{n-1}^{Z+1}}{\Delta r}\right)+\dot{q}_n \tag{17}$$

Multiply Eq. (17) by Δt and divide by $\rho_c C_c$ resulted to:

$$T_n^{Z+1}-T_n^Z=\frac{3K_{c(n^+)}r_{n^+}^2\Delta t}{\rho_{c(m)}C_{c(m)}\Delta r\left(r_{n^+}^3-r_{n^-}^3\right)}\left[T_{n+1}^{Z+1}-T_n^{Z+1}\right]- \frac{3K_{c(n^-)}r_{n^-}^2\Delta t}{\rho_{c(m)}C_{c(m)}\Delta r\left(r_{n^+}^3-r_{n^-}^3\right)}\left[T_n^{Z+1}-T_{n-1}^{Z+1}\right]+\frac{3\Delta t\dot{q}_n}{\rho_{c(m)}C_{c(m)}} \tag{18}$$

$$\therefore T_n^Z+\frac{3\Delta t\dot{q}_n}{\rho_{c(m)}C_{c(m)}}=T_n^{Z+1}-\left[\frac{3K_{c(n^+)}r_{n^+}^2\Delta t}{\rho_{c(m)}C_{c(m)}\Delta r\left(r_{n^+}^3-r_{n^-}^3\right)}\right]\left[T_{n+1}^{Z+1}\right]+ \left[\frac{3K_{c(n^+)}r_{n^+}^2\Delta t}{\rho_{c(m)}C_{c(m)}\Delta r\left(r_{n^+}^3-r_{n^-}^3\right)}\right]\left[T_n^{Z+1}\right]+\left[\frac{3K_{c(n^-)}r_{n^-}^2\Delta t}{\rho_{c(m)}C_{c(m)}\Delta r\left(r_{n^+}^3-r_{n^-}^3\right)}\right]\left[T_n^{Z+1}\right]+ \left[\frac{3K_{c(n^-)}r_{n^-}^2\Delta t}{\rho_{c(m)}C_{c(m)}\Delta r\left(r_{n^+}^3-r_{n^-}^3\right)}\right]\left[T_{n-1}^{Z+1}\right] \tag{19}$$

Collecting the like terms from Eq. (19) yielded:

$$\therefore T_n^Z+\frac{3\Delta t\dot{q}_n}{\rho_{c(m)}C_{c(m)}}=\left[\left(\frac{3\Delta t}{\rho_{c(m)}C_{c(m)}\Delta r}\right)\frac{K_{c(n^-)}r_{n^-}^2}{\left(r_{n^+}^3-r_{n^-}^3\right)}\right]\left[T_{n-1}^{Z+1}\right]+ \left[1+\left\{\left(\frac{3\Delta t}{\rho_{c(m)}C_{c(m)}\Delta r}\right)\frac{\left(K_{c(n^-)}r_{n^-}^2+K_{c(n^+)}r_{n^+}^2\right)}{\left(r_{n^+}^3-r_{n^-}^3\right)}\right\}\right]\left[T_n^{Z+1}\right]- \left[\left(\frac{3\Delta t}{\rho_{c(m)}C_{c(m)}\Delta r}\right)\frac{K_{c(n^+)}r_{n^+}^2}{\left(r_{n^+}^3-r_{n^-}^3\right)}\right]\left[T_{n+1}^{Z+1}\right] \tag{20}$$

This resulting equation is valid for any general, interior node within the globe-shaped concrete $0 < r_n < R$.

At the center node, where $r_n = 0$ the temperature profile is axisymmetric, and $\frac{\partial T}{\partial r} = 0,$ when $r = 0$ thus, the temperature on either side of the node is equal.

$$T_{n-1}^{Z+1} = T_{n+1}^{Z+1}$$

$$likewise, K_{c(n^-)} = K_{c(n^+)}$$

∴Eq. (20) simplified to:

$$\therefore T_n^Z + \frac{\Delta t \dot{q}_n}{\rho_{c(m)} C_{c(m)}} = T_n^{Z+1} - \left(\frac{6\Delta t}{\rho_{c(m)} C_{c(m)} \Delta r^2} K_{c(n^+)} \right) T_{n+1}^{Z+1} \tag{21}$$

This occur at $r_n = 0$.

This simplified form of Eq. (20) was used to represent the center node.

The conduction through the surface of the globe-shaped concrete is equal to the convection at the surface.

$$\therefore -K \frac{\partial T}{\partial r}_{at,\, r=R} = -U_C (T_{r=R} - T_\infty) \tag{22}$$

However, this boundary condition cannot be directly represented in finite difference form, since such formulation requires a volume element and Eq. (22) applies at a point.

Instead a first law energy balance was utilized to obtain the nodal equation for the surface of the globe-shaped concrete. This energy balance can be written as:

$$\dot{E}_{in} - \dot{E}_{out} + \dot{E}_{gen} = \dot{E}_{st} \tag{23}$$

where,

$$\dot{E}_{in} = -KA \frac{\partial T}{\partial r} \tag{24}$$

$$\dot{E}_{out} = U_C A \left(T - T_g \right) \tag{25}$$

$$\dot{E}_{gen} = \dot{q} V \tag{26}$$

$$\dot{E}_{st} = \rho C V \frac{\partial T}{\partial t} \tag{27}$$

Representing Eq. (23) in a finite difference form consistent with Eq. (20) and (21) resulted to:

$$-KA \frac{\partial T}{\partial r} - U_C A \left(T - T_g \right) + \dot{q} V = \rho C V \frac{\partial T}{\partial t} \tag{28}$$

This can be written in finite difference form to give:

$$\begin{aligned} &-4\pi r_{n^-}^2 K_{n^-} \frac{T_n^{Z+1} - T_{n-1}^{Z+1}}{\Delta r} - 4\pi r_n^2 U_C \left(T_n^{Z+1} - T_\infty \right) + \frac{4}{3} \pi \left(r_n^3 - r_{n^-}^3 \right) \dot{q}_n = \\ &\frac{4}{3} \pi \rho C_n \left(r_n^3 - r_{n^-}^3 \right) \frac{T_n^{Z+1} - T_n^Z}{\Delta t} \end{aligned} \tag{29}$$

where, U_c = convection coefficient.

Solving for T_n^Z plus known quantities involving $\dot{q}$ and U_c, in a similar manner to Eq. (20) and (24) resulted to:

$$\frac{-4\pi r_{n^-}^2 K_{n^-} T_n^{Z+1}}{\Delta r} + \frac{-4\pi r_{n^-}^2 K_{n^-} T_{n-1}^{Z+1}}{\Delta r} - 4\pi r_n^2 U_C T_n^{Z+1} - 4\pi r_n^2 U_C T_\infty + \frac{4}{3}\pi\left(r_n^3 - r_{n^-}^3\right)\dot{q}_n = \frac{4}{3}\pi\rho C_n \frac{\left(r_n^3 - r_{n^-}^3\right)}{\Delta t} T_n^{Z+1} - \frac{4}{3}\pi\rho C_n \frac{\left(r_n^3 - r_{n^-}^3\right)}{\Delta t} T_n^Z \tag{30}$$

Multiply Eq. (30) by Δt and divide by $\frac{4}{3}\pi\rho\left(r_n^3 - r_{n^-}^3\right)$ resulted to:

$$T_n^Z - T_n^{Z+1} = \frac{3\Delta t}{\Delta r \rho C_n}\left(\frac{r_{n^-}^2 K_{n^-}}{r_n^3 - r_{n^-}^3}\right) T_n^{Z+1} - \frac{3\Delta t}{\Delta r \rho C_n}\left(\frac{r_{n^-}^2}{r_n^3 - r_{n^-}^3}\right) T_{n-1}^{Z+1} + \frac{3\Delta t U_C}{\rho C_n}\left(\frac{r_{n^-}^2}{r_n^3 - r_{n^-}^3}\right) T_n^{Z+1} + \frac{3\Delta t U_C}{\rho C_n}\left(\frac{r_n^2}{r_n^3 - r_{n^-}^3}\right) T_\infty - \frac{\dot{q}_n \Delta t}{\rho C_n} \tag{31}$$

$$T_n^Z + \frac{\Delta t}{\rho C_n}\dot{q}_n + \frac{3\Delta t U_C}{\rho C_n}\left(\frac{r_{n^-}^2}{r_n^3 - r_{n^-}^3}\right) = -\left(\frac{3\Delta t}{\Delta r \rho C_n}\frac{r_{n^-}^2 K_{n^-}}{r_n^3 - r_{n^-}^3}\right) T_{n-1}^{Z+1} + \left[1 + \frac{3\Delta t}{\rho C_n \Delta r}\left(\frac{r_{n^-}^2 K_{n^-}}{r_n^3 - r_{n^-}^3}\right) + \frac{3\Delta t U_C}{\rho C_n}\left(\frac{r_n^2}{r_n^3 - r_{n^-}^3}\right)\right] T_n^{Z+1} \tag{32}$$

$$T_n^Z = -\left(\frac{3\Delta t}{\Delta r \rho C_n}\frac{r_{n^-}^2 K_{n^-}}{r_n^3 - r_{n^-}^3}\right) T_{n-1}^{Z+1} + \left[1 + \frac{3\Delta t}{\rho C_n \Delta r}\left(\frac{r_{n^-}^2 K_{n^-}}{r_n^3 - r_{n^-}^3}\right) + \frac{3\Delta t U_C}{\rho C_n}\left(\frac{r_n^2}{r_n^3 - r_{n^-}^3}\right)\right] T_n^{Z+1} - \frac{\Delta t}{\rho C_n}\dot{q}_n - \frac{3\Delta t U_C}{\rho C_n}\left(\frac{r_{n^-}^2}{r_n^3 - r_{n^-}^3}\right) \tag{33}$$

Eqs. (20), (21) (32) and (33) constitute a system of algebraic equations for heat transfer modeling in globe-shaped concrete.

4. Result and discussion

The values of Eq. (33) are obtained from the values in **Table 1**. Since the thermal properties are constant, average temperatures could therefore be used to determine thermal properties of bed materials.

The following data were obtained from the theoretical/mathematical modeling carried out on thermal performance of packed bed energy storage system as shown in **Figure 3**.

The following are the definitions of the symbols:

Time = the interval time of measurements, in minutes.

$\mathbf{T_{s\text{-}in}}$ = the inlet air temperature to the packed bed storage tank in °C.

$\mathbf{T_{s\text{-}out}}$ = the outlet air temperature from the packed bed storage tank in °C.

Parameters	Values
Airflow rate	0.01316 m^3/s (28 cfm)
Air—density	1.07154 Kg/m^3
Air—specific heat capacity	1008 J/Kg K
Concrete—density	2400 Kg/m^3
Concrete—specific heat capacity	1130 J/Kg K
Copper tube—density	8900 Kg/m^3
Copper tube—specific heat capacity	384 J/Kg K
Area of globe-shaped concrete	0.013 m^2
Area of copper tube + header	0.664 m^2
Volumetric heat transfer coefficient	106.5 W/m^3 K

Table 1. Modeling parameters.

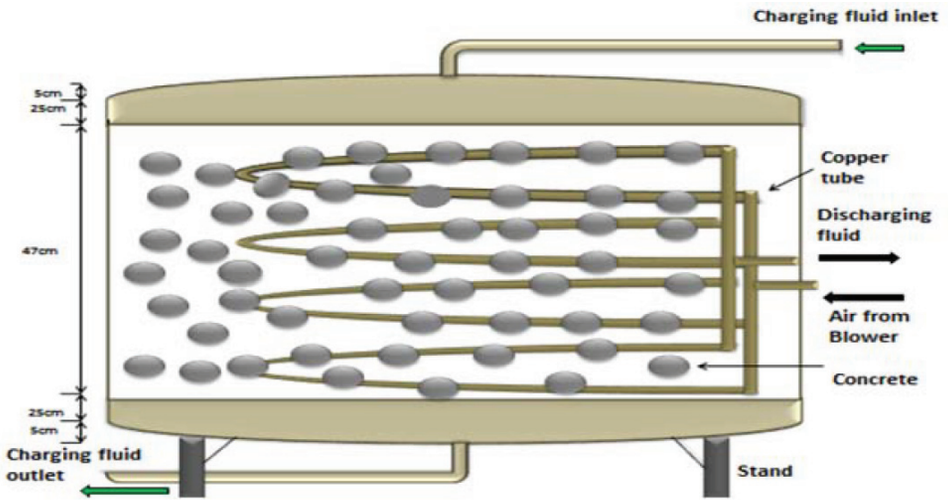

Figure 3. Schematic of the storage tank systems.

$\mathbf{T_{t\text{-}in}}$ = the inlet air temperature to the copper tube in °C.

$\mathbf{T_{t\text{-}out}}$ = the outlet air temperature from the copper tube in °C.

$\mathbf{T_{A1}}$, $\mathbf{T_{A2}}$, $\mathbf{T_{A3}}$, **and** $\mathbf{T_{A4}}$ = the air stream temperatures (°C) through the bed at different heights of the storage tank 117.5, 235, 352.5, and 470 cm, respectively.

$\mathbf{T_{ci1}}$, $\mathbf{T_{ci2}}$, $\mathbf{T_{ci3}}$, **and** $\mathbf{T_{ci4}}$ = the core temperatures of the globe-shaped concrete (°C) through the bed at different heights of the storage tank 117.5, 235, 352.5, and 470 cm, respectively.

$\mathbf{T_{ti1}}$, $\mathbf{T_{ti2}}$, $\mathbf{T_{ti3}}$, **and** $\mathbf{T_{ti4}}$ = the temperatures of air flowing inside the copper tube (°C) through the bed at different heights of the storage tank 117.5, 235, 352.5, and 470 cm, respectively.

T_{ct1}, T_{ct2}, T_{ct3}, and T_{ct4} = the temperatures of the contact made between globe-shaped concrete and imbedded copper tube (°C) through the bed at different heights of the storage tank 117.5, 235, 352.5, and 470 cm, respectively.

T_{t1}, T_{t2}, T_{t3}, and T_{t4} = the surface temperatures of the copper tube (°C) through the bed at different heights of the storage tank 117.5, 235, 352.5, and 470 cm, respectively.

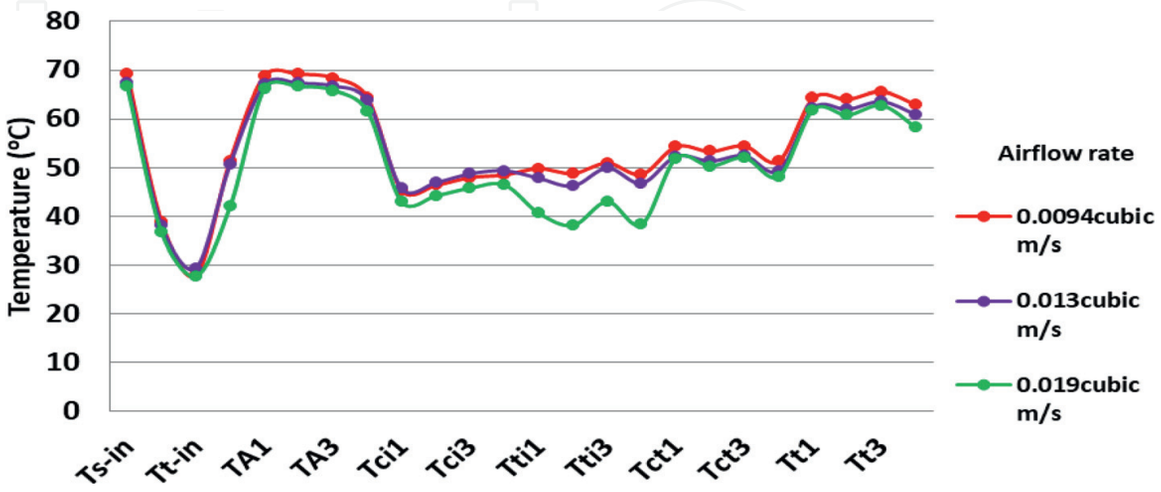

Figure 4. Average temperature measurement of charging packed bed storage system for globe-shaped concrete of size 0.11 m diameter and flow rate of 0.0094, 0.013, and 0.019 m^3/s.

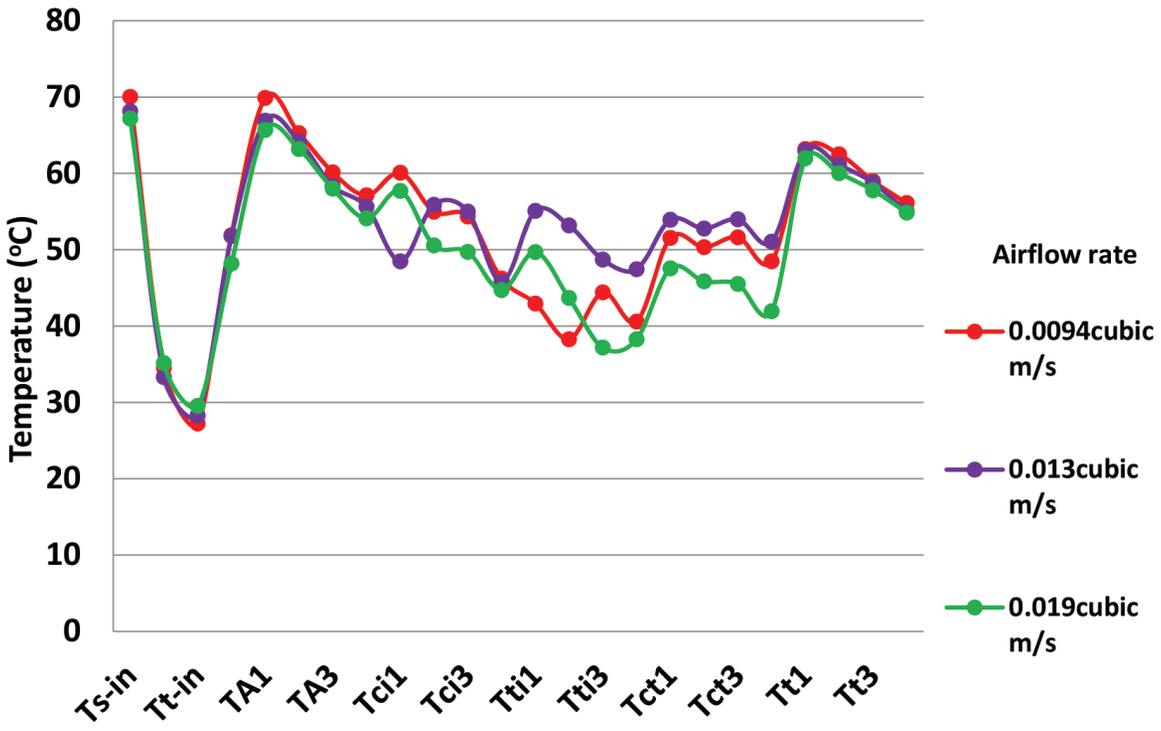

Figure 5. Average temperature measurement of charging packed bed storage system for globe-shaped concrete of size 0.08 m diameter and flow rate of 0.0094, 0.013, and 0.019 m^3/s.

The results of the experimentation were shown in **Figures 4–6** for globe-shaped concrete of size 0.11; 0.08 and 0.065 m diameter respectively while the discharging only temperature measurements were shown in **Figures 7–9** respectively for air flow rate of 0.0094, 0.013, and 0.019 m^3/s.

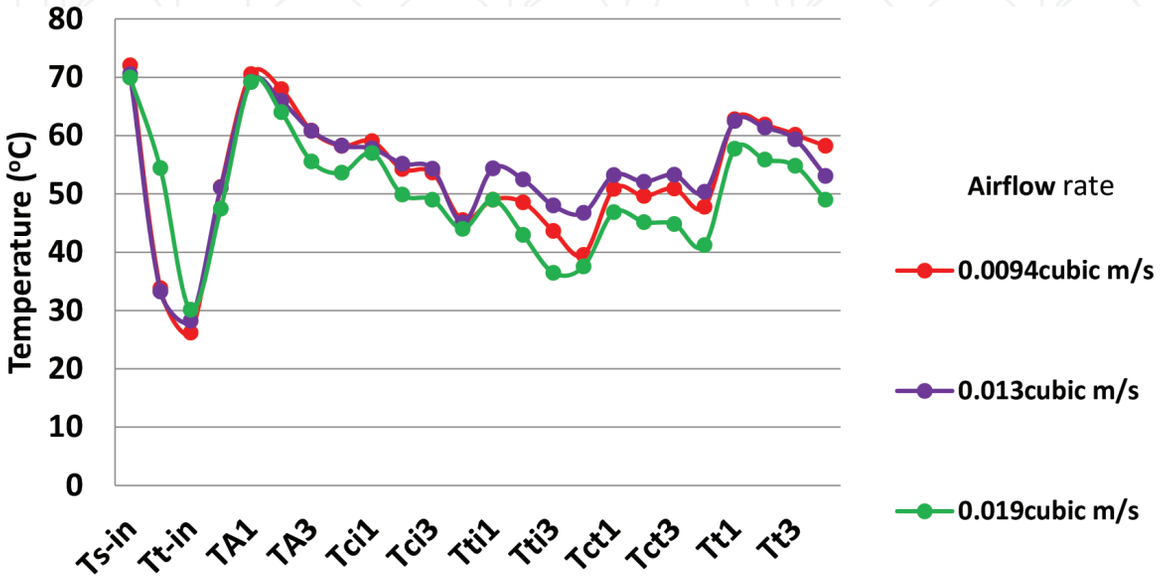

Figure 6. Average temperature measurement of charging packed bed storage system for globe-shaped concrete of size 0.065 m diameter and flow rate of 0.0094, 0.013, and 0.019 m^3/s.

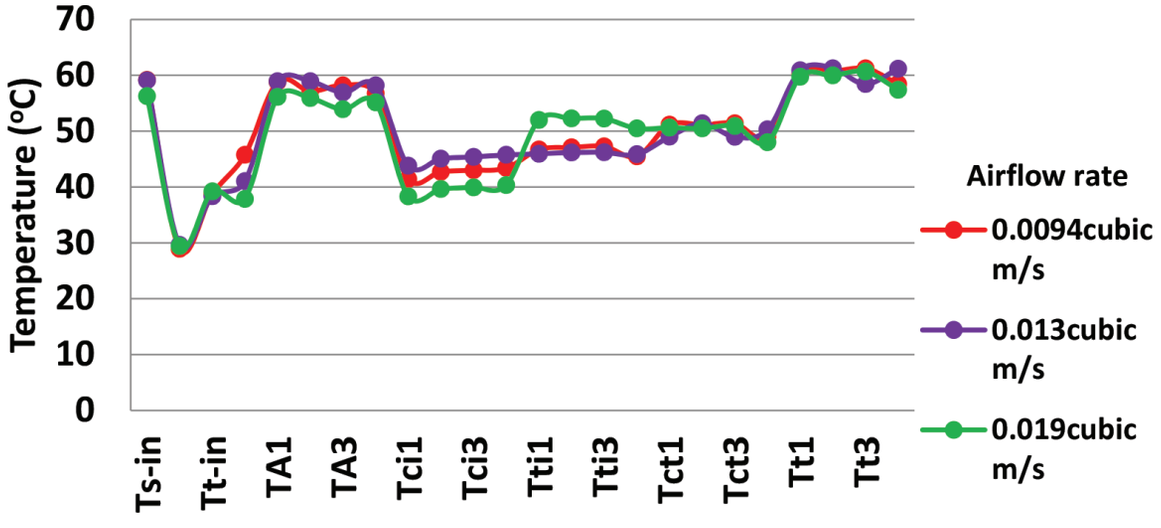

Figure 7. Average temperature measurement of discharging packed bed storage system for globe-shaped concrete of size 0.11 m diameter and flow rate of 0.0094, 0.013, and 0.019 m^3/s.

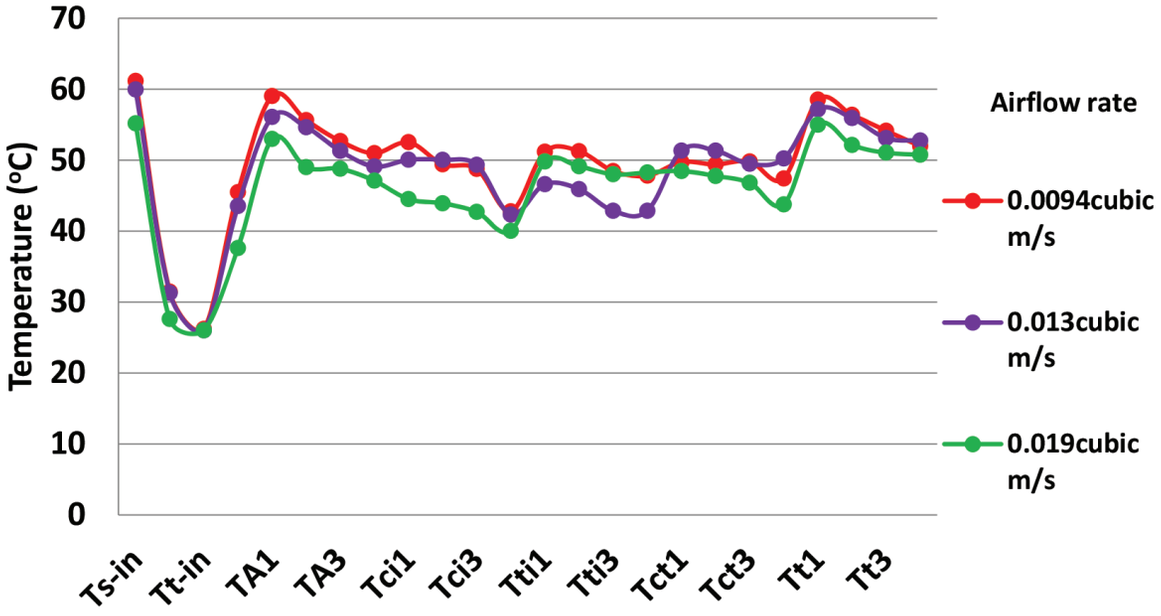

Figure 8. Average temperature measurement of discharging packed bed storage system for globe-shaped concrete of size 0.08 m diameter and flow rate of 0.0094, 0.013, and 0.019 m^3/s.

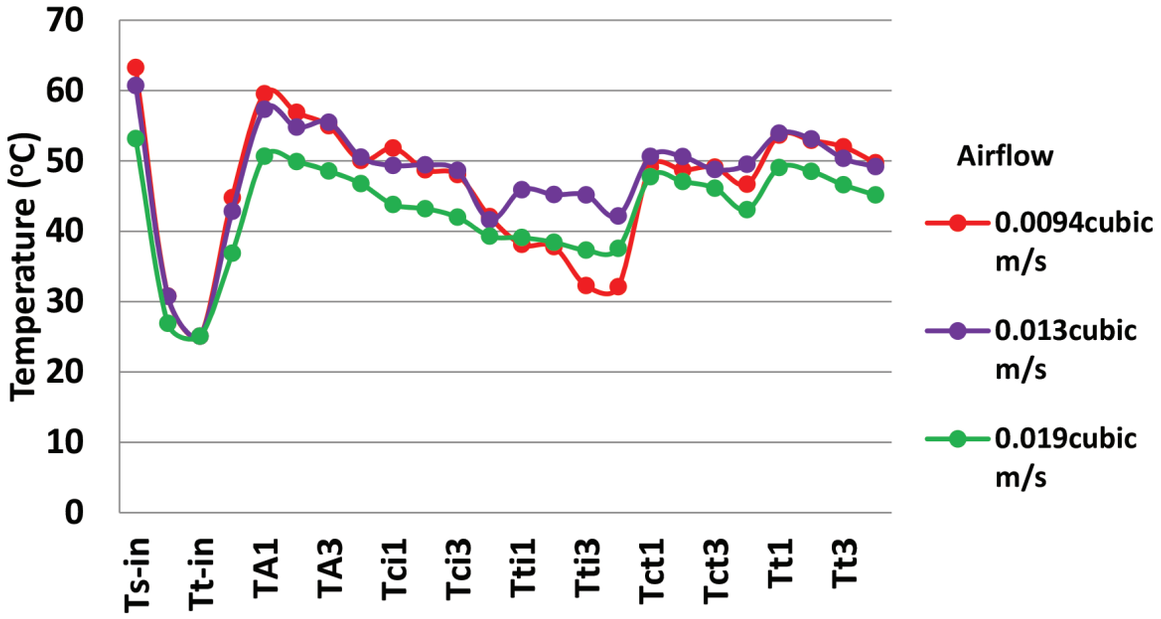

Figure 9. Average temperature measurement of discharging packed bed storage system for globe-shaped concrete of size 0.065 m diameter and flow rate of 0.0094, 0.013, and 0.019 m^3/s.

Figure 10 presents the comparison of the temperature variations with time at Ts-in, $T_{s\text{-}out}$, $T_{t\text{-}in}$, $T_{t\text{-}out}$, T_{A1}, T_{A2}, T_{A3}, T_{A4}, T_{ci1}, T_{ci2}, T_{ci3}, T_{ci4}, T_{ti1}, T_{ti2}, T_{ti3}, T_{ti4}, T_{ct1}, T_{ct2}, T_{ct3}, T_{ct4}, T_{t1}, T_{t2}, T_{t3}, and T_{t4} during the simultaneous charging and discharging while **Figure 11** presents for discharging only. The comparisons were presented for air flow rates of 0.0094, 0.013, and 0.019 m^3/s.

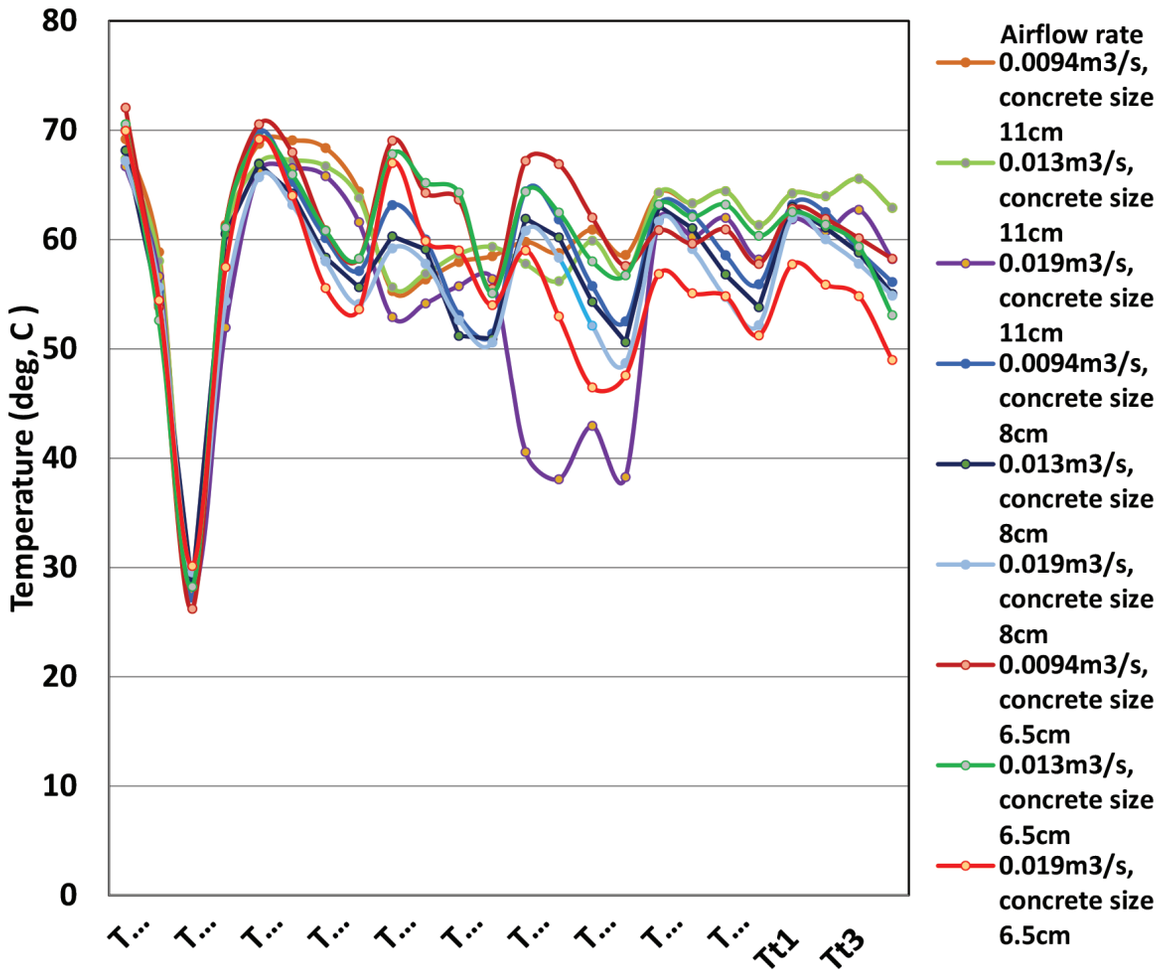

Figure 10. Comparison of average temperature measurement of charging packed bed storage system for globe-shaped concrete of size 0.065, 0.08, 0.11 m in diameter and flow rate of 0.0094, 0.013, and 0.019 m^3/s.

These figures show that the difference of the temperature response between the charging and fluid to solid heat transfer process at the initial period (<30 min) of the packed bed was large (large inlet–outlet temperature difference means large heat supply), and the heat recovered by the cool air (approximately 27°C) flowing inside the copper tube was fairly high (larger inlet–outlet temperature difference compared with the later period indicates larger heat recovery).

Therefore, a relatively large part of the heat supplied by the simulated air heater was used to heat the air flowing inside the copper tube through conduction and convection and also stores the rest for continuous usage.

The following are the storage efficiency for globe-shaped concrete of size 0.11 m, 0.08 m and 0.065 m diameter at airflow rate of 0.0094, 0.013 and 0.019 m^3/s (**Figure 12**):

For 0.11 m diameter globe-shaped concrete:

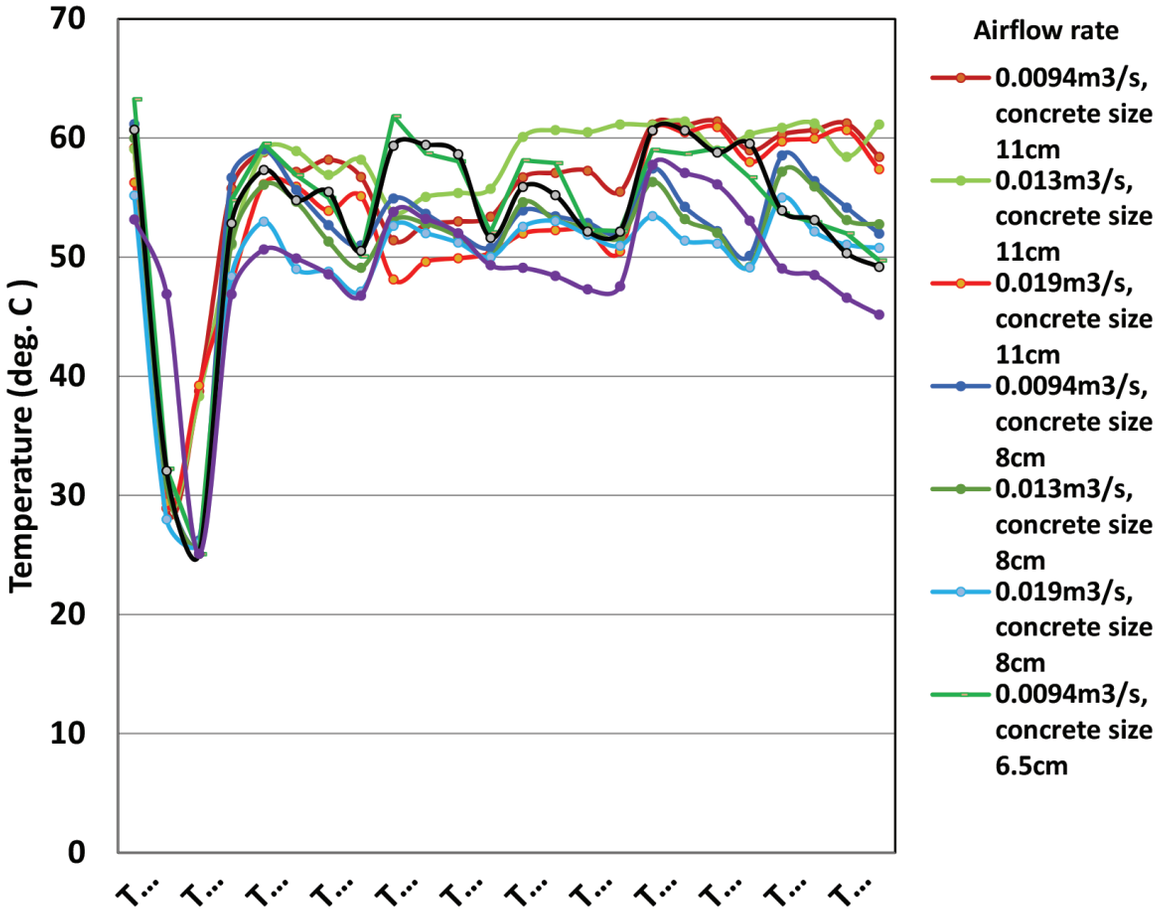

Figure 11. Comparison of average temperature measurement of discharging packed bed storage system for globe-shaped concrete of size 0.065, 0.08, 0.11 m in diameter and flow rate of 0.0094, 0.013, and 0.019 m^3/s.

i. Storage efficiency at air flow rates of 0.0094 m^3/s = 40.7%

ii. Storage efficiency at air flow rates of 0.013 m^3/s = 60.5%

iii. Storage efficiency at air flow rates of 0.019 m^3/s = 57.5%

For 0.08 m diameter globe-shaped concrete:

i. Storage efficiency at air flow rates of 0.0094 m^3/s = 23.5%

ii. Storage efficiency at air flow rates of 0.013 m^3/s = 51.3%

iii. Storage efficiency at air flow rates of 0.019 m^3/s = 50.2%

For 0.065 m diameter globe-shaped concrete:

i. Storage efficiency at air flow rates of 0.0094 m^3/s = 14.8%

ii. Storage efficiency at air flow rates of 0.013 m^3/s = 35.06%

iii. Storage efficiency at air flow rates of 0.019 m^3/s = 40.3%

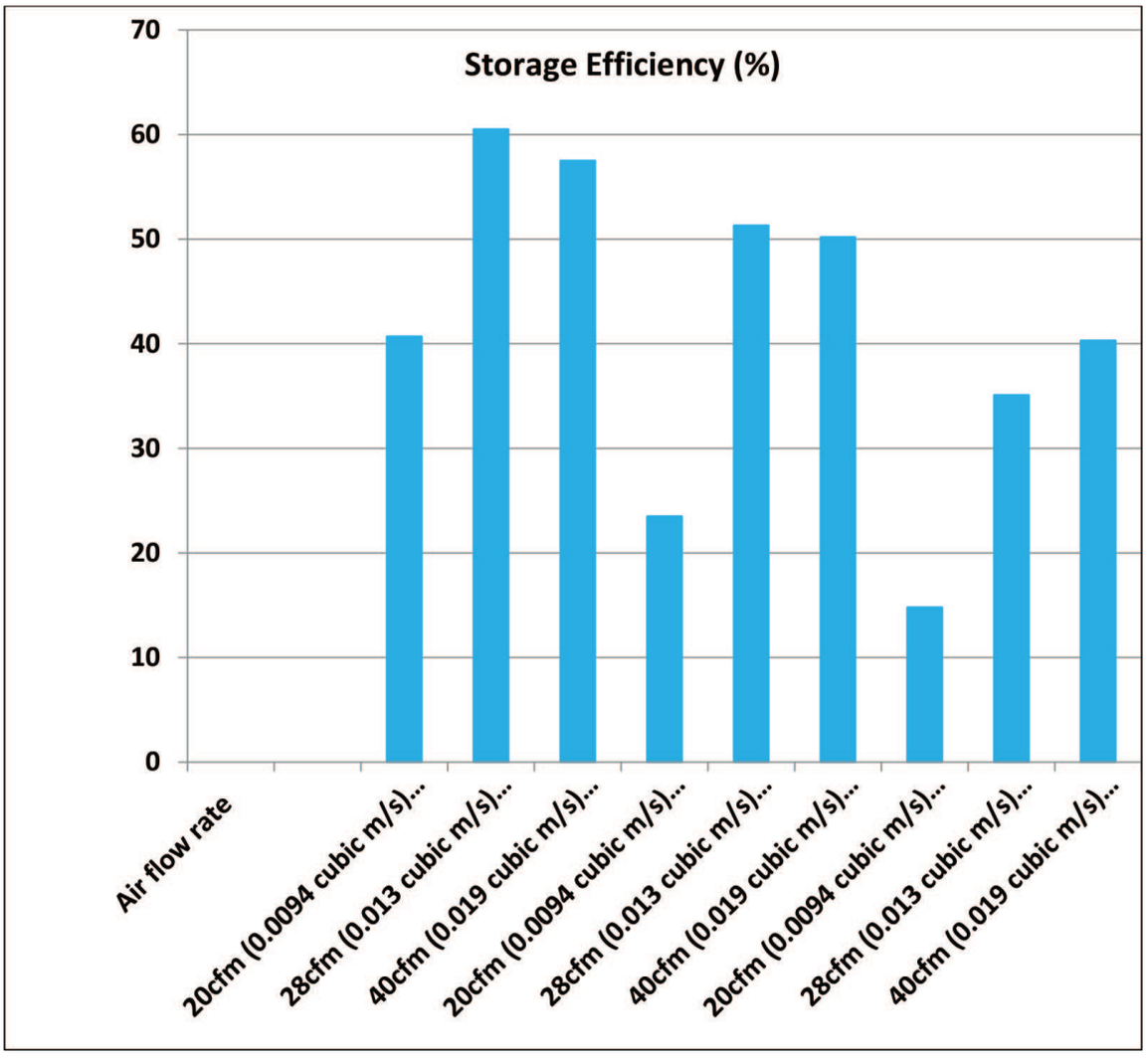

Figure 12. Storage efficiency of simultaneous charging and discharging packed bed storage system for globe-shaped concrete of diameter 0.065, 0.08, 0.11 m and air flow rate 0.0094, 0.013, and 0.019 m^3/s.

5. Conclusion

The study led to the following findings and conclusions:

1. The mathematical model developed can accurately predict the temperature within the concrete bed for energy storage purpose.
2. The steady intermittent input temperature variation actually led to continuous discharge temperature at the copper tube outlet.
3. The mathematical model may be extended to specify the packed bed storage system dimensions.
4. Globe-shaped concrete of 0.11 m diameter has the highest storage efficiency of 60.5% at 0.013 m^3/s airflow rate.

Author details

Adeyanju Anthony Ademola

Address all correspondence to: anthony.adeyanju@sta.uwi.edu

Mechanical and Manufacturing Engineering Department, University of the West Indies, St. Augustine, Trinidad and Tobago

References

[1] Adeyanju AA, Manohar K. Theoretical and experimental investigation of heat transfer in packed beds. Research Journal of Applied Sciences. 2009;**4**(5):166-177

[2] Balakrishnan AR, Pei DCT. Heat transfer in fixed bed. In: Industrial and Engineering Chemical Process Design Development. Vol. 13. Washington DC, USA: ACS Publication; 1974. pp. 441-446

[3] Anzelius A. 1926. Heating by means of percolating media. Journal of Mechanical and Agriculture, ASAE, 41st ed 6:291-296. AE 1996

[4] Schumann TEW. Heat transfer: A liquid flowing through a porous prism. Journal of Heat Transfer. 1929;**5**:208-212

[5] Furnas CC. Heat transfer from a gas stream to a bed of broken solids. Journal of Chemical Engineering. 1930;**22**:26-721

[6] Saunders OA, Ford. Heat transfer in the flow of gas through a bed of solid particles. Journal of Iron and Steel. 1940;**141**:291-296

[7] Kays WM, London AC. Compact Heat Exchangers. New York: McGrawHILL; 1964

[8] Löf GOG, Hawley RW. Unsteady state heat transfer between air and loose solids. Journal of Industrial Engineering. 1948;**40**(6):1061-1070

[9] Leva M, Grummer M. Concentration and temperature profiles in a tubular reactor. Industrial and chemical engineering fundamental. ACS Publication. 1948;**40**:747-753

[10] Riaz M. Analytical solution for single and two phase models of packed bed thermal storage systems. Journal of Heat Transfer. 1977;**99**:489-492

[11] Jefferson CP. Prediction of break through curves in packed beds: Applicability of single parameter models. AlChE Journal. 1972;**18**(2):409-416

[12] Ball WE. Heat transfer properties of a packed bed: Determination by a frequency response technique [Dissertation Abstract], Vol. **19**; 1958. p. 494

[13] Norton CL. Pebble heater: New heat transfer unit for industry. Journal of the American Ceramic Society. 1946;**29**:187-193

[14] Meek RMG. The measurement of heat transfer coefficients in packed beds by the cyclic method. In: International Heat Transfer Development. New York, USA: ASME; 1961

[15] Bradshaw RC, Myers JE. Heat and mass transfer in fixed and fluidized beds of large particles. AIChE Journal. 1963;**9**:590-599

[16] Harker JH, Martyn EJ. Energy storage in gravel beds. Journal of the Institute of Energy. 1985;**58**:94-99

[17] Bouguettaia H, Harker JH. Energy storage in packed beds of spheres containing palm oil. Journal of the Institute of Energy. 1991;**64**:89-94

[18] Lanz JE. A numerical model of thermal effects in a microwave irradiated catalyst bed [M.Sc. thesis]; Virginia, USA: Virginia Polytechnic Institute and State University; 1998